Evidence for charge localization in the ferromagnetic phase of $La_{1-x}Ca_xMnO_3$ from high real-space-resolution x-ray diffraction

S. J. L. Billinge, Th. Proffen, and V. Petkov
Department of Physics and Astronomy and Center for Fundamental Materials Research, Michigan State University, East Lansing, Michigan 48824-1116

J. L. Sarrao
Los Alamos National Laboratory, Los Alamos, New Mexico 87545

S. Kycia
Cornell High Energy Synchrotron Source, Ithaca, New York 14853
(Received 21 July 1999; revised manuscript received 11 January 2000)

High real-space-resolution atomic pair distribution functions of $La_{1-x}Ca_xMnO_3$ ($x=0.12$, 0.25, and 0.33) have been measured using high-energy x-ray powder diffraction to study the size and shape of the MnO_6 octahedron as a function of temperature and doping. In the paramagnetic insulating phase we find evidence for three distinct bond lengths which we ascribe to Mn^{4+}-O, Mn^{3+}-O-short, and Mn^{3+}-O-long bonds, respectively. In the ferromagnetic metallic (FM) phase, for $x=0.33$ and $T=20$ K, we find a single Mn-O bond length; however, as the metal-insulator transition is approached either by increasing T or decreasing x, intensity progressively appears around $r=2.15$ and in the region 1.85−1.9 Å suggesting the appearance of Mn^{3+}-O-long bonds and short Mn^{4+}-O bonds. This is strong evidence that charge localized and delocalized phases coexist close to the metal-insulator transition in the FM phase.

I. INTRODUCTION

The importance of the lattice to the colossal magnetoresistance (CMR) phenomenon[1] is now fairly well established.[2–7] There is a strong electron-lattice coupling due to the Jahn-Teller effect which affects Mn^{3+} ions[2,8] and the doped carriers tend to localize as small polarons at high temperature and low doping.[4–6,9–15] However, exact agreement about the detailed nature of local Jahn-Teller (JT) and polaronic distortions is lacking. This information is important for separating competing models describing the CMR phenomenon.

Early diffraction,[5] atomic pair distribution function[4] (PDF), and extended x-ray absorption fine structure[6,16] (XAFS) studies demonstrated that atomic disorder, measured as the Mn-O bond-length distribution, increases as samples pass through the metal-insulator (MI) transition with temperature. This is qualitatively what is expected if polarons are forming as the sample enters the insulating phase. These techniques also agree that the onset of polaron formation is gradual with temperature, taking place over a temperature range of 50–100 K below the MI transition temperature T_m. In general, PDF (Refs. 4,9,17) and XAFS (Refs. 6,16,18) results suggest that in CMR materials the local structure is significantly different from that observed crystallographically. In particular, Mn-O_6 octahedra can have a significant JT distortion locally even when globally the average JT distortion is zero or negligible. Although the local structural studies agree on this point there is disagreement on the amplitude of the distortions, in particular the length of the long JT bond. For instance, Louca *et al.*[9,17] propose, based on the observation of a persistent negative fluctuation[19] in the neutron PDFs of $La_{1-x}Sr_xMnO_3$ at around 2.2−2.3 Å, that this is the length of the JT long bond. This seems surprising given that the JT long-bond in the undoped material is shorter at 2.18 Å.[20] On the other hand, XAFS measurements of the Ca doped system[6] suggest that the JT long bond is between 2.1–2.2 Å and a difference modeling of the neutron PDF from the $La_{1-x}Ca_xMnO_3$ system[4] supports these findings, as we discuss below.

Another question which is not resolved is the nature of the charge ground-state of the ferromagnetic metallic (FM) phase. Local density approximation calculations suggest that a delocalized charge state would not have any JT distortion even when the e_g band is not completely empty. Thus, the ferromagnetic metallic state, which we refer to as the Zener state (following Radaelli[21]), would have regular undistorted octahedra. The observation of essentially undistorted MnO_6 octahedra at low temperature in the FM phase is supported by XAFS (Ref. 16) and PDF results at high enough doping (away from the low-temperature MI transition). However, there has been a prediction based on XAFS data that small octahedral distortions persist at low temperature in the FM phase suggesting that the ground state is a large polaron state.[18] PDF data have also been interpreted in terms of a three-site polaron model[9] at low temperature persisting at least up to a doping level of $x=0.3$. It is important to determine the ground state of the FM phase.

Other interesting phenomena also take place in the FM phase when the MI transition is approached as a function of temperature or doping. Upon increase in temperature structural distortions start to appear in the local structure below T_c.[4–6] They also appear when, at low temperature, doping is decreased towards $x=0.17-0.18$.[9,17] In the vicinity of the MI transition the FM phase does not seem to be in a pure

Zener state. The exact nature of this inhomogeneous state is, however, not fully characterized.

We have undertaken a high real-space resolution x-ray PDF study of the $La_{1-x}Ca_xMnO_3$ system to try and resolve some of the issues discussed above. Specifically, by applying the PDF technique we would like to study the distribution of Mn-O distances in a series of manganites to elucidate the nature of the charge ground state of the FM phase: i.e., is it fully delocalized or not. We would like to investigate what is the nature of the local Jahn-Teller and polaronic distortions in this material and how they evolve as a function of doping and temperature. Finally, we would like to differentiate between the competing models for the evolution of the charge state away from the ground-state as the MI transition is approached as a function of temperature and doping.

By definition, the atomic pair distribution function PDF is the instantaneous atomic density-density correlation function which describes the atomic arrangement in materials.[22] It is the sine Fourier transform of the experimentally observable structure factor obtained in a powder diffraction experiment.[23] Since the total structure function includes both the Bragg intensities and diffuse scattering its Fourier associate, the PDF, yields both the local and average atomic structure of materials. By contrast, an analysis of the Bragg scattering intensities alone yields only the average crystal structure. Determining the PDF has been the approach of choice for characterizing glasses, liquids and amorphous solids for a long time.[23,24] However, its wide spread application to crystalline materials, such as manganites, where some local deviation from the average structure is expected to take place, has been relatively recent.[25]

We chose to use high-energy x rays to measure the PDFs because it is possible to get high-quality data at high-Q values (Q is the magnitude of the wave vector) allowing accurate high real-space resolution PDFs to be determined.[26] It was previously thought that neutrons were superior for high-Q measurements because, as a result of the Q dependence of the x-ray atomic form factor the x-ray coherent intensity gets rather weak at high Q; however, the high flux of x rays from modern synchrotron sources more than compensates for this and we have shown that high quality high-resolution PDFs can be obtained using x rays.[26]

II. EXPERIMENTAL

The $La_{1-x}Ca_xMnO_3$ samples were synthesized by standard solid-state reaction. Stoichiometric amounts of La_2O_3, $CaCO_3$, and MnO_2 were mixed with a mortar and pestle and placed in an alumina crucible. The material was fired at 1050, 1300, and 1350 °C for one day each with intermediate grindings. After the final grinding, the material was fired at 1400 °C for an additional day and then slow-cooled over 20 h to room temperature. Samples were characterized by conventional powder x-ray diffraction, temperature-dependent magnetization, and electrical resistivity.

Synchrotron powder diffraction experiments were carried out at the A2 24 pole wiggler beam line at Cornell High Energy Synchrotron Source (CHESS). This beam line is capable of delivering an intense beam of high-energy x rays required for high resolution PDF measurements. Data were collected in symmetric transmission geometry. The polychromatic incident beam was dispersed using a Si (111) monochromator and x rays of energy 61 keV ($\lambda = 0.203$ Å) were used. An intrinsic Ge detector coupled to a multichannel analyzer was used to detect the scattered radiation, allowing us to extract the coherent component of the scattered x-ray intensities by setting appropriate energy windows. The diffraction spectra were collected by scanning at constant Q steps of $\Delta Q = 0.025$ Å^{-1}. Multiple scans up to $Q_{max} = 40$ Å^{-1} were conducted and the resulting spectra averaged to improve the statistical accuracy and reduce any systematic error due to instability in the experimental setup. The data were normalized for flux, corrected for background scattering and experimental effects such as detector deadtime and absorption. The part of the Compton scattering at low values of Q not eliminated by the preset energy window was removed analytically applying a procedure suggested by Ruland.[27] The resulting intensities were divided by the average atomic form factor for the sample to obtain the total structure factor $S(Q)$

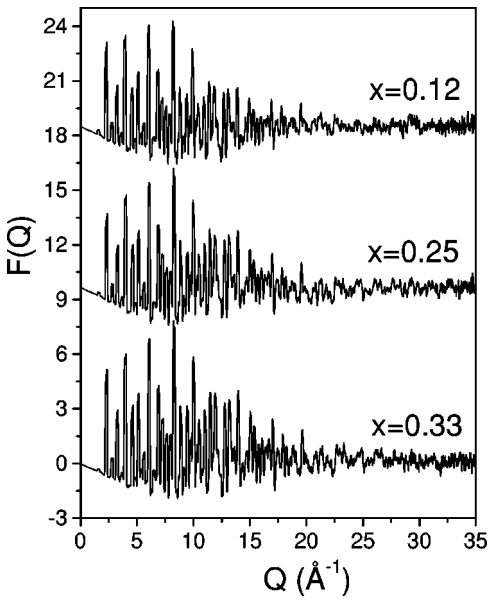

FIG. 1. Reduced structure factors $F(Q) = Q[S(Q) - 1]$ for $La_{1-x}Ca_xMnO_3$, $x = 0.12$, 0.25, and 0.33, measured at 20 K. The function $F(Q)$ oscillates around zero and the individual data sets are offset for clarity.

$$S(Q) = 1 + \frac{I_c(Q) - \Sigma_i c_i f_i^2(Q)}{[\Sigma_i c_i f_i]^2}, \tag{1}$$

where I_c is the measured coherent part of the spectrum, c_i and $f_i(Q)$ are the atomic concentration and scattering factor of the atomic species of type i (i=La, Ca, Mn, and O), respectively.[28] All data processing procedures were carried out using the program RAD.[29] The measured reduced structure factors $F(Q) = Q[S(Q) - 1]$ for $x = 0.12$, 0.25, and 0.33 at $T = 20$ K are shown in Fig. 1. The data are terminated at $Q_{max} = 35$ Å^{-1} beyond which the signal to noise ratio became unfavorable. Note that this a very high wave vector for x-ray diffraction measurements; for example, a conventional Cu $K\alpha$ x-ray source has a Q_{max} of less than 8 Å^{-1}. The corresponding reduced atomic distribution functions $G(r)$, obtained via Fourier transform

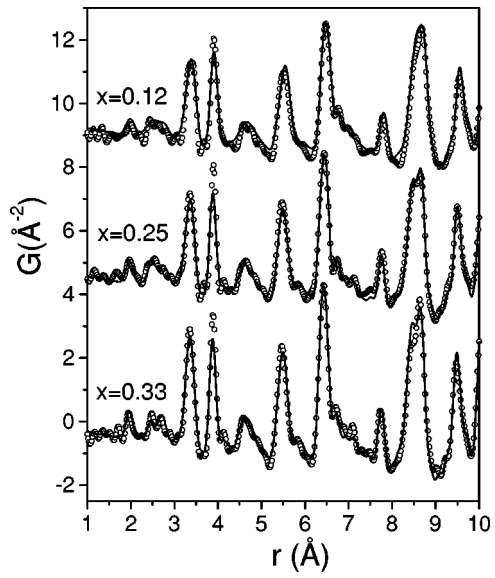

FIG. 2. Reduced radial distribution functions $G(r)$, for $La_{1-x}Ca_xMnO_3$, $x=0.12$, 0.25, and 0.33 at 20 K are shown as open circles. The corresponding fits are displayed as solid lines (see text for details). The function $G(r)$ oscillates around zero and the individual data sets are offset for clarity.

$$G(r)=\frac{2}{\pi}\int_0^\infty Q[S(Q)-1]\sin(Qr)dQ, \tag{2}$$

are shown as open circles in Fig. 2. Additional room temperature data of samples with $x=0.12$ and $x=0.33$ were taken at the bending magnet beamline BM1 at the Advanced Photon Source (APS). The experimental setup was similar to the one used at CHESS apart from a slightly higher energy of 65 KeV being used at APS. The data processing to obtain the PDF was identical for both experiments.

III. RESULTS

A. Polarons versus JT distortion

For the sake of clarity we would like to define the terminology we will use in the following discussion. There are two types of octahedral distortions which are observed in manganites. The first is a quadrupolar symmetry elongation of the MnO_6 octahedron i.e., it has two long Mn-O bonds and four shorter Mn-O bonds. This is associated with the presence of a Mn^{3+} ion and is referred to as a Jahn-Teller distortion.[30] Another possible distortion is an isotropic breathing-mode collapse of the MnO_6 octahedron where a regular octahedron stays regular (six equal bond lengths) but the octahedron shrinks. This type of distortion can be associated with the presence of a Mn^{4+} ion.[4] We refer to this as a polaronic distortion since the Mn^{4+} ions appear only when doped holes become localized.

We note that in the literature the Jahn-Teller distorted octahedra are often referred to as ''Jahn-Teller polarons.''[7,31,32] We avoid this terminology because the presence of Jahn-Teller distorted octahedra need not imply the presence of polarons in the sense of localized doped holes; for example, the undoped $LaMnO_3$ compound is fully Jahn-Teller distorted but contains no doped holes.[33,20] While it can be argued that these are polarons because the Jahn-Teller distortion splits the e_g band making this compound insulating it confuses the discussion of the state, localized or delocalized, of the doped holes. In our discussion we confine the use of ''polaron'' to describe a *doped hole* localized with an associated lattice distortion.

These doped-hole polarons have also been described in the literature as ''anti-Jahn-Teller polarons.''[17,34] This terminology comes about when one considers what happens when a doped hole localizes in a background of Jahn-Teller distorted Mn^{3+} octahedra, for example, in the lightly doped region of the phase diagram. On the site where the hole localizes the Jahn-Teller distortion is locally destroyed; thus the name. Again, we avoid this terminology because it is not appropriate when the polaronic state is approached from the delocalized ferromagnetic metallic state (the Zener state). In this case, as we discuss below, there are initially no Jahn-Teller distorted octahedra. The octahedra are regular and conform to those seen in the average crystal structure. As the metal-insulator transition is approached the doped holes begin to localize. When they localize both breathing mode collapsed doped-hole polarons (Mn^{4+}) *and* Jahn-Teller distorted sites (Mn^{3+}) *are created*. From this perspective it seems confusing to think of the polarons as ''anti-Jahn-Teller'' polarons. This also raises the point that, while we are not calling the Jahn-Teller distorted octahedra polarons, in the heavily doped material the presence of fully Jahn-Teller distorted octahedra implies the presence of localized Mn^{4+} polarons and vice versa.

B. Comparison to the crystal structure

First we compare the present experimental PDFs to the average crystal structure determined by other independent studies. Experimental PDFs were fit with the crystallographic model.[35] The refinement was done using the program PDFFIT.[36] Lattice parameters, isotropic thermal parameters, and atomic positions were refined conserving the symmetry of the space group ($Pbnm$). The calculated PDFs corresponding to the best fit are shown in Fig. 2 as solid lines. Inspection of the figure shows a satisfactory agreement between the calculated and measured PDFs for all three compositions which shows that the present experimental PDFs are, in general, consistent with the average crystal structure of doped manganites. Furthermore, the values refined reproduce the Rietveld found values very well. The rather large difference observed for the PDF peak at $r\approx 4.0$ Å is believed to be related to dopant ion effects on the La/Ca site. Attempts to model these differences are currently under way.

Local structural deviations from the average structure will show up as deficiencies in the agreement since the fits were constrained so the model has the average structure. We are particularly interested in the size and shape of the *local* MnO_6 octahedron; we therefore concentrate on the low-r region of the PDF. An enlarged view of the region around the nearest-neighbor Mn-O distance is shown in Fig. 3. The experimental data are shown as open circles. Two model PDFs are shown: The solid line represents the PDF of the refined average structural model for doped manganites. Although the average structure is orthorhombic, the difference in the three distinct Mn-O bond lengths is very small making the MnO_6 octahedra virtually regular. The dotted line is the

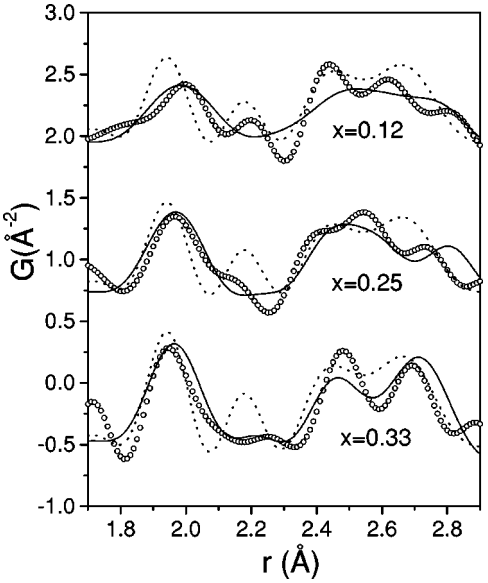

FIG. 3. Low r region of the data (open circles) and refinements (solid line) shown in Fig. 2 and calculated PDFs for a structural model showing full JT distortions on all sites are shown as dotted lines. See text for more details.

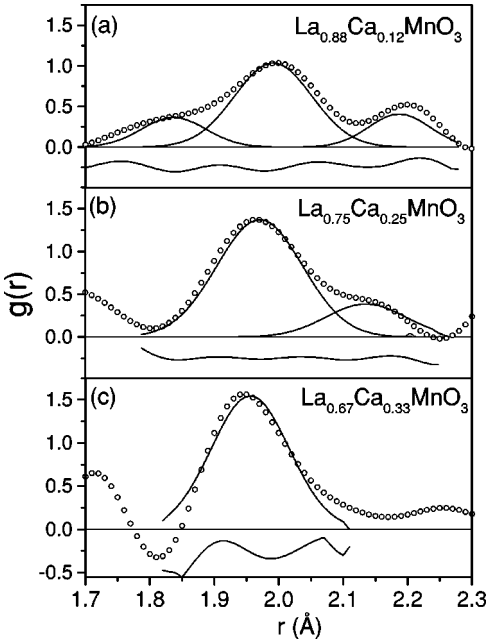

FIG. 4. Low-r region of the PDF on an expanded scale from $x=0.12$, 0.25, and 0.33 at 20 K (open circles). Solid lines are Gaussian fits to the data. The function $g(r)$ which is plotted is defined as $g(r)=1+G(r)/4\pi r\rho_0$ where ρ_0 is the number density of the material.

PDF calculated from the average structure of *undoped* $LaMnO_3$ where all Mn-O octahedra have a large JT distortion, i.e., short and long Mn-O bonds are present. These are clearly resolved in the calculation.[20] All the model curves are convoluted with the experimental real-space resolution function of the data which comes from the finite Q range of the data.

It is apparent from Fig. 3 that the model based on the average structure fits the $x=0.33$ and 0.25 data quite well in this low-r region but less well in the $x=0.12$ data set. In fact, in the $x=0.12$ data the dashed line representing the JT distorted octahedra does a qualitatively better job of reproducing the shape of the Mn-O bonds in the region 2.0−2.5 Å and the shape of the second neighbor multiplet around 2.4–2.8 Å. This supports the idea that, locally, large JT distortions persist in the insulating phase although these do not show up in the average crystal structure. In the ferromagnetic metallic phase ($x=0.25$ and 0.33) the local structure is much closer to the average crystal structure.

C. Low-temperature structure of the MnO_6 octahedra

We now focus on the region of the PDF from $1.7\leqslant r\leqslant 2.3$ Å containing the peaks from the MnO_6 octahedra. This region is shown on an expanded scale in Fig. 4 for doping levels $x=0.12$, 0.25, and 0.33 at 20 K. The procedure we use to extract information from this region of the PDF $g(r)$ is fitting Gaussians to the data. The bond lengths are then given by the peak positions of the fitted Gaussians. The resulting values are affected by random errors such as noise in the data and systematic errors such as the uncertainty in the x-ray wavelength. For the low-r region discussed in this, and the following section, we estimate the determined bond lengths have a rather large uncertainty of ± 0.03 Å. This large uncertainty comes about because of the low signal-to-noise ratio and the limited range of the fit. Note that for the refinement of the complete PDF of the $x=0.33$ sample at $T=20$ K (Fig. 3), we find a Mn-O bond length with an accuracy of $\Delta r=\pm 0.007$ Å. We are fitting this narrow range because we want to understand the size and shape of the MnO_6 octahedra and fitting a wider range obscures this information.

We are interested to know how the MnO_6 octahedron evolves as a function of doping. At $x=0.33$ the first PDF peak is fit with a single Gaussian. There is a suggestion of peak asymmetry, but there is negligible intensity in the region above 2.1 Å. This single Gaussian fit means that all six Mn-O bonds have almost the same length of $r=1.96$ Å at $x=0.33$ and $T=20$ K. This is what would be expected for a fully delocalized charge state.

The PDF for $x=0.25$ sample clearly has intensity on the high-r side of its first peak at 1.95 Å which has been fit with a second Gaussian component. The presence of intensity at this $r=2.15$ Å position remains invariant as $Q_{\max}$ is varied (although the resolution of the feature changes). This suggests that it is real and not artificial since noise artifacts and termination ripples change position and intensity as $Q_{\max}$ is varied. The suggestion is, therefore, that even at $T=20$ K and $x=0.25$ long Mn-O bonds and, therefore, residual Jahn-Teller distorted sites persist in the material. There is no direct evidence for intensity on the low-r side of the main 1.95 Å peak although it does not decrease as sharply as the $x=0.33$ sample.

The $x=0.12$ sample is in the insulating state and is expected to be fully localized and polaronic. In this case we see three components to the peak and have fit it with three Gaussians. At this composition there exist nominally Mn^{3+} octahedra which are Jahn-Teller distorted. Based on the structure of undoped $LaMnO_3$, we expect these to have four short bonds at 1.92–1.96 Å and two long bonds at 2.18 Å.

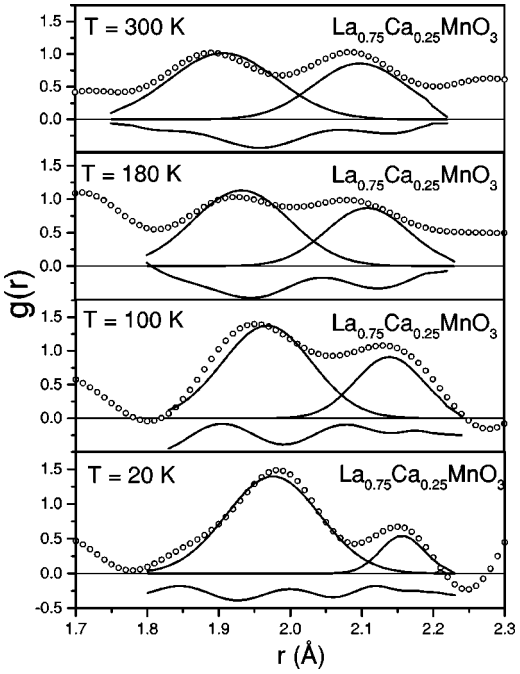

FIG. 5. Low-r region of the PDF on an expanded scale from $x=0.25$ at 20, 100, 180, and 300 K (open circles). Solid lines are Gaussian fits to the data. Even at the lowest temperature $T=20$ K a contribution at the position of the JT long bond can be observed which increases as the temperature is increased.

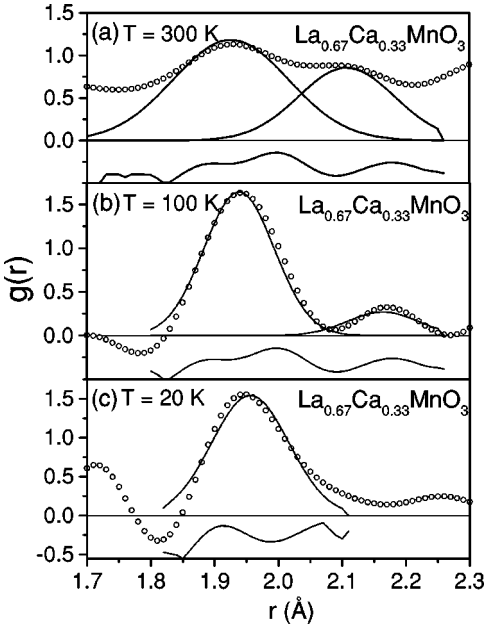

FIG. 6. Low-r region of the PDF on an expanded scale from $x=0.33$ at 20, 100, and 300 K (open circles). The solid lines are Gaussian fits to the data. Here no contribution at the position of the JT long bond is observed at $T=20$ K, however, is appears as the temperature is raised to $T=100$ K and further to room temperature.

The two higher-r components of the peak seem consistent with this allocation. The intensity on the low-r side might then be expected to originate from the Mn^{4+} polaronic sites. This is consistent with the prediction of the breathing mode model[4] which suggests short polaronic bonds of <1.9 Å, and is also consistent with the crystal chemistry of Mn^{4+}. Based on Shannon's ionic radii[37] the expected Mn^{4+}(VI)-O^{2-}(II) ionic radius is 1.88 Å. This short Mn-O bond length is also found in the material $CaMnO_3$ (Ref. 38) where all Mn sites are nominally Mn^{4+}. It appears clear that Mn^{4+} polarons exist with bonds $\leqslant 1.9$ Å together with Mn^{3+} sites which have a JT distortion which is similar to that in the undoped material.

D. Temperature dependence of the MnO_6 octahedra

We now concentrate on the temperature evolution of MnO_6 octahedra using the same procedure as described in the last section. In Fig. 5 we show the evolution of the PDF peaks around $r=2.0$ Å as a function of temperature between $T=20$ K and $T=300$ K for the $x=0.25$ sample. The temperature dependence of the same region in r for the sample with $x=0.33$ is shown in Fig. 6. The metal-insulator (MI) transition for the $x=0.25$ sample is at $T=235$ K and at $T=280$ K for $x=0.33$. As we discussed in the previous section, at low temperature a large central peak centered around 1.97 Å is evident with a small high-r component at 2.15 Å. As temperature is raised, the intensity in the high-r component increases. It is dangerous to infer a bond length directly from the position of a maximum in the data because of the influence of noise on these data. The small intensity of these peaks is evident in Fig. 2 and noise contamination can cause a peak intensity to be shifted somewhat. However, the presence or absence of intensity at some position is a robust result. It is clear that the intensity grows in the region $r=2.1$–2.15 Å and below 1.9 Å. It is also apparent that there is no intensity above 2.2 Å suggesting that the JT long bond is $\sim 2.15-2.18$ Å. Since the sample at room temperature is in the insulating state we expect to observe a Mn^{4+}-O short bond as for the $x=0.12$ sample at $T=20$ K. However, inspection of Fig. 5 only shows a shift of intensity of the peak at ~ 1.95 Å to lower r. This can be taken as evidence of the Mn^{4+}-O short bond, since the PDF peaks at higher temperatures are significantly broader due to thermal motion making it impossible to resolve the two short Mn-O bonds.

Next we look how the PDF of the MnO_6 octahedron of the $x=0.33$ sample evolves with temperature. This is shown in Fig. 6. At low temperature this sample exhibited a single peak centered at 1.96 Å. There is no evidence of any JT long-bond. At 100 K clear evidence of a component of intensity at $r=2.18$ Å appears. The central peak also comes down less steeply on the low-r side and the peak centroid is shifted somewhat to lower-r which suggest that some intensity is appearing on the low-r side of the peak. Finally at room temperature we clearly see significant intensity at the position of the JT long bond. Again the peaks are broadened due to thermal motion compared to the PDF at $T=20$ K. In summary for both $x=0.25$ and $x=0.33$, as the temperature is increased towards the MI transition, the low-r peak shifts slightly to the left and intensity appears around $r=2.15$ Å.

IV. DISCUSSION

The ability to collect high-quality data at high values of the wave vector Q using high-energy synchrotron radiation has allowed us to decompose the bond length distribution of

the MnO_6 octahedra into its components more reliably than was previously possible with neutrons. This is well demonstrated by the fact that the present PDF data are consistent with the structure models derived by independent Rietveld studies and, furthermore, produce physically reasonable values for the short Mn^{4+} and the short and long Mn^{3+} bonds.

The measured x-ray scattering intensity corresponds to a snapshot of the atomic arrangement and the resulting PDF gives the instantaneous atomic density-density correlation function. For example, x-ray PDFs have been used to measure correlated atomic motion,[39] which indicates that the PDF is instantaneous on typical phonon time scales. From our data it is not possible to tell whether the distortions we observe are static or dynamic in origin.

We draw the following conclusions from our results described above. If we assume that the $x=0.12$ sample is fully localized in the polaronic state at 10 K, as is suggested by by its exponential resistivity,[4,11,12] we can interpret the three components of the first peak in the PDF as being due to JT distorted Mn^{3+} octahedra and regular but contracted Mn^{4+} octahedra. If we assume the number of doped holes p to be the nominal Ca concentration x, then we expect the number of 1.88 Å bonds to be $6p=6x=0.72$. The number of JT distorted sites will be $(1-p)=(1-x)$. Then, if we assume that the JT distorted Mn^{3+} octahedra have essentially four short and two long bonds with average lengths 1.95 and 2.18 Å, as observed in the undoped material,[20,40] we expect a peak with intensity $4(1-x)=3.52$ at 1.95 Å and $2(1-x)=1.76$ at 2.18 Å. To test whether our data support this polaron model, we compare this prediction with our data. Fitting the first peak in the experimental PDF with Gaussians [Fig. 4(a)] yields subcomponents with intensity ratios of 1.0(5):4.0(5):1.0(5) centered at 1.84, 1.96, and 2.18 Å (the corresponding values for the model are 0.72:3.52:1.76 at 1.88, 1.95, and 2.18 Å). Since our estimate of the uncertainty in bond-length from these Gaussian fits is ± 0.03 Å, this result represents a reasonable agreement, providing some confidence to this interpretation.

We would like now to expand on the interplay between the polaron formation and the existence of JT distortions in the manganites studied. A simple picture could be constructed as follows: There are no distorted Mn-O octahedral units in the delocalized Zener phase and all Mn-O bond-lengths in the MnO_6 octahedron are ~ 1.97 Å, as found in the average crystal structure. This is the case observed at $x=0.33$ and $T=20$ K so that the sample may be considered to be in fully delocalized charge state. In the insulating phase there coexist small, regular Mn^{4+} octahedra with six Mn-O bonds of $\sim 1.85-1.9$ Å and Jahn-Teller distorted Mn^{3+} octahedra with four bonds of ~ 1.97 Å and two bonds of $2.1-2.15$ Å length. This is the picture which we see at $x=0.12$, $T=20$ K and at $x=0.25$ and $x=0.33$ at $T=300$ K (see Figs. 4, 5, and 6). All of these samples are in the insulating phase and the charge carriers, as the measured Mn-O bond length distributions suggest, are essentially fully localized. This observation of a long JT bond in the range of $2.1-2.15$ Å agrees with our own neutron data and those of Hibble *et al.*[41] but not with the work of Louca *et al.*[17]

Within the FM phase but at intermediate temperatures, and compositions approaching the MI transition, we see evidence for JT-long bonds appearing (see Fig. 7). This suggests that there is a coexistence of localized Jahn-Teller phase and delocalized Zener phase material. The sample is still conducting because the regions of Zener phase percolate. This is similar to the picture emerging for the MI transition in $La_{0.625-y}Pr_yCa_{0.375}MnO_3$ which occurs as a function of x,[42] although the length-scale of the inhomogeneities is much smaller in this case and were also suggested for the MI transition in $La_{1-x}Sr_xMnO_3$ system.[17]

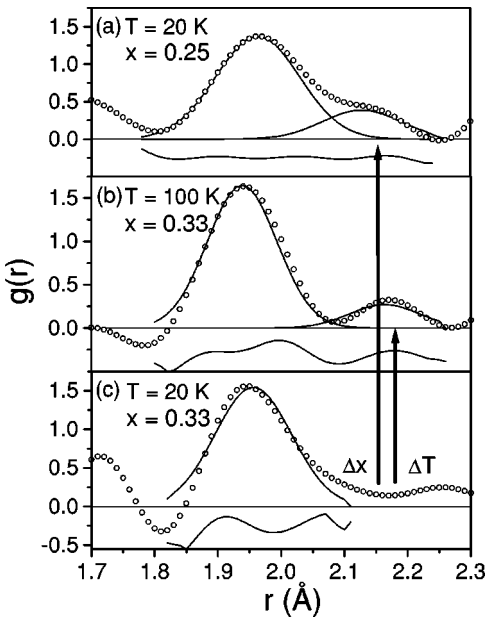

FIG. 7. Low-r region of the PDF on an expanded scale from $x=0.33$ at 20, and 300 K and for $x=0.25$ at 20 K (open circles). The solid lines are Gaussian fits to the data. The arrows mark the crossing of the MI phase transition as function of $x(\Delta x)$ and temperature (ΔT).

Our picture is consistent with the earlier observation of a breathing mode distortion on one-in-four manganese sites which set in below the MI transition in $La_{0.79}Ca_{0.21}MnO_3$.[4] This was found to reproduce the changes in the local structure which occur at the MI transition in this sample when the amplitude of the collapse was $\delta=0.12$ Å. Since the starting value of the Mn-O bond-length at low temperature before the distortion set in was 1.97 Å this results in short Mn^{4+} bonds of 1.85 Å shorter than, but similar to, what we observe here. Furthermore, because the model was evaluated at the special composition of $x=0.25$, this breathing mode collapse coincidentally resulted in Jahn-Teller-like distortions on *all* the remaining Mn sites with Mn^{3+}-long bonds of $1.97+0.12=2.09$ Å. This is illustrated schematically in Fig. 8. This model gives a very satisfactory agreement with the current results given its simplicity. We do not wish to imply here that the breathing mode collapse causes the Jahn-Teller distortion; merely that they coexist in the localized phase and that there is good consistency between the earlier neutron data and the current x-ray data.

It is interesting to note from Fig. 8 that $x=0.25$ is a special composition where small polarons can form an ordered lattice separated by JT distorted Mn^{3+} sites which are unstrained. Each Mn^{4+} site has six neighboring Mn^{3+} sites whose long-bonds point towards it and these complexes fit together into a space filling three-dimensional (3D) network. There is no experimental evidence that polarons order in this

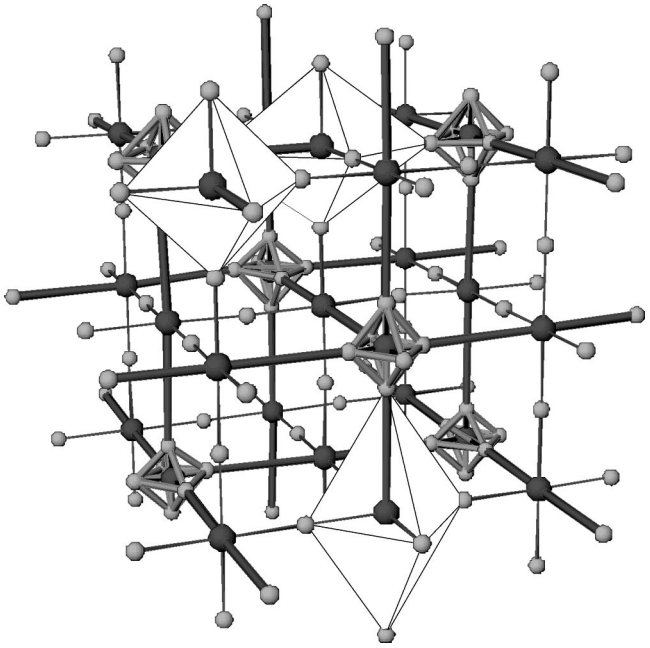

FIG. 8. Ordered polaron model for $x=0.25$. The small octahedra are on 1/4 of the sites and contain localized Mn^{4+} ions. The other Mn sites (large balls) have elongated JT distorted octahedral coordination whose long-bonds are represented by thick lines. These can be oriented along *x*, *y*, or *z* and always point towards a polaron. Three of the octahedra have been drawn in to illustrate this fact. For clarity the magnitude of the polaronic–Jahn-Teller distortions are exaggerated.

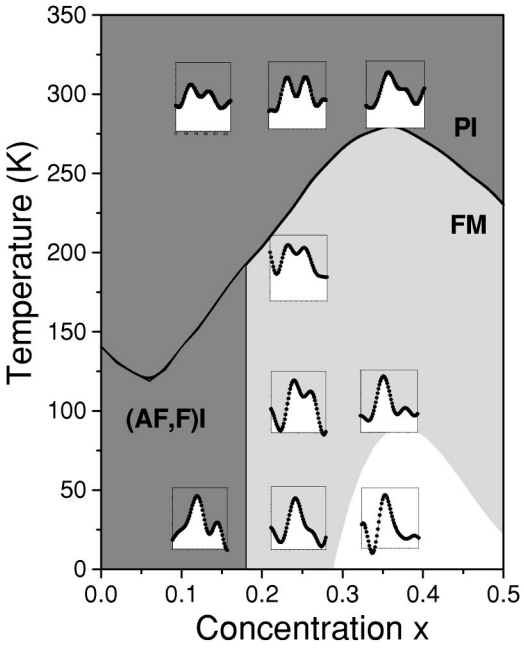

FIG. 9. Schematic phase diagram for $La_{1-x}Ca_xMnO_3$. The solid lines are electronic and magnetic transitions taken from Refs. 43 and 44. I and M refer to insulating and metallic respectively and P, F, and AF to paramagnetic, ferromagnetic, and antiferromagnetic. Superimposed on the figure are the low-*r* PDF peaks showing the MnO_6 octahedra. In the insulating phases the JT long bond is clearly apparent. There is no JT long bond deep in the FM phase; however, it gradually appears as the MI boundary is approached. The shading signifies coexistence of charge localized and delocalized phases and the white area is the fully charge delocalized region. The light shading indicates metallic behavior.

way in this system; rather charge stripes are observed.[43] However, this model does show how orbitals can order locally around an Mn^{4+} defect site to minimize strain. Such an ''orbital polaron'' has been predicted theoretically.[45]

So far, we have shown that by studying the size and shape of the MnO_6 octahedra we can determine whether the charge is localized as small polarons (observation of 1.88 and 2.18 Å Mn-O bonds in the PDF) or delocalized (observation of a single Mn-O bond length ~ 1.97 Å). These two states are exemplified by the $x=0.12$ sample at 20 K [Fig. 4(a)] and the $x=0.33$ sample at 20 K [Fig. 6(c)] respectively. As the temperature is increased below T_c in the $x=0.33$ and $x=0.25$ samples, significant components of the long and short bonds become evident. This suggests that carriers are becoming localized in parts of the sample. The high-resolution PDF data therefore support the idea of an inhomogeneous sample with charge delocalized metallic regions of Zener phase coexisting with regions of charge localized JT phase. As T_c is approached from below the amount of charge localized phase increases at the expense of the charge delocalized phase as evidenced by the growth of intensity in the regions $1.85-1.9$ Å and $2.1-2.15$ Å on increasing temperature in the $x=0.25$ sample (Fig. 5). This view is consistent with Booth *et al.*'s interpretation of their XAFS data[6,16] and the interpretation of our earlier neutron PDF data.[4,46] The MI transition and the onset of long-range ferromagnetic order presumably coincides with the percolation of the Zener phase. This is similar to the original proposition that the MI transition was a percolation transition by Louca *et al.*,[17] though our data support the idea that the Zener phase percolates rather than a network of connected three-site polarons.

A number of theories predict charge phase separation[47] or two-fluid behavior[48] of the charge system. We note that our data is entirely consistent with the coexistence of delocalized Zener phase and localized JT phase below T_c but does not directly imply the existence of charge segregation between these phases; rather it is just the state of localization of the charges which differs in the different regions of the sample,[46] as is proposed for $La_{0.625-y}Pr_yCa_{0.375}MnO_3$.[42]

Finally, we address the issue of how the charge state evolves as the MI transition is approached as a function of doping *x*. As the experimental data suggest for $x=0.33$ and $T=20$ K no polaronic or JT distortions are present, i.e., the true ground-state of the FM metallic phase is a completely delocalized Zener state. Although we have a sparse data-set one can notice the similarity of the Mn-O bond length distributions for $x=0.33$ at 100 K and $x=0.25$ at 20 K (see Fig. 7). Thus, as one moves away from the ground state a localized state appears that coexists with the delocalized one. The volume of the localized state increases as the MI transition is approached, whether as a function of temperature (see Fig. 5 and 6) or doping (see Fig. 4). The MI transition itself then occurs when the proportion of delocalized phase is too small to percolate. This view is summarized in Fig. 9. In this figure the first peaks in the experimental PDFs, reflecting the MnO_6 octahedral bond length distribution, are plotted at the positions on the phase diagram where they were measured. The shading signifies coexistence of charge localized and delocalized phases and the white area is the fully charge delocal-

ized region. The light shading indicates metallic behavior. The positions of the MI transitions are taken from standard phase diagrams of this system.[43,44]

V. CONCLUSIONS

Using the PDF analysis of high energy x-ray diffraction we can distinguish the charge localized and charge delocalized states of $La_{1-x}Ca_xMnO_3$ ($x=0.12$, 0.25, 0.33). We characterize the nature of the polaronic distortion around Mn^{4+} as being an isotropic octahedron with Mn-O bond length of $\sim 1.88-1.9$ Å. The FM phase is only homogeneous at low temperature and high doping above $\sim x=0.3$. As temperature is raised or doping lowered towards the MI transition the FM state becomes inhomogeneous with a coexistence of localized JT phase and delocalized Zener phase.

ACKNOWLEDGMENTS

We would like to thank J. D. Thompson and M. F. Hundley for help in characterizing the samples, Matthias Gutmann for help with data collection, and E. Božin for a critical reading of the manuscript. Our gratitude extends to S. D. Shastri for helping with the data collection at APS. We would like to acknowledge stimulating discussions with P. G. Radaelli. This work was supported by the NSF through Grant No. DMR-9700966 and by the Alfred P. Sloan Foundation. CHESS was funded by NSF through Grant No. DMR97-13424 and APS by the US DOE through Grant No. W-31-109-Eng-38.

[1] A.P. Ramirez, J. Phys.: Condens. Matter **9**, 8171 (1997).
[2] A.J. Millis, P.B. Littlewood, and B.I. Shraiman, Phys. Rev. Lett. **74**, 5144 (1995).
[3] H. Röder, J. Zang, and A.R. Bishop, Phys. Rev. Lett. **76**, 1356 (1996).
[4] S.J.L. Billinge, R.G. DiFrancesco, G.H. Kwei, J.J. Neumeier, and J.D. Thompson, Phys. Rev. Lett. **77**, 715 (1996).
[5] P. Dai, J. Zhang, H.A. Mook, S.-H. Liou, P.A. Dowben, and E.W. Plummer, Phys. Rev. B **54**, R3694 (1996).
[6] C.H. Booth, F. Bridges, G.J. Snyder, and T.H. Geballe, Phys. Rev. B **54**, R15 606 (1996).
[7] G. Zhao, K. Conder, H. Keller, and K.A. Müller, Nature (London) **381**, 676 (1996).
[8] J.R. Fletcher and K.W.H. Stephens, J. Phys. C **2**, 444 (1969).
[9] D. Louca, T. Egami, E.L. Brosha, H. Röder, and A.R. Bishop, Phys. Rev. B **56**, R8475 (1997).
[10] P. Schiffer, A.P. Ramirez, W. Bao, and S.-W. Cheong, Phys. Rev. Lett. **75**, 3336 (1995).
[11] G.M. Jonker and J.H. van Santen, Physica (Utrecht) **16**, 337 (1950).
[12] M. Jaime, M.B. Salamon, M. Rubinstein, R.E. Treece, J.S. Horwitz, and D.B. Chrisey, Phys. Rev. B **54**, 11 914 (1996).
[13] T.T.M. Palstra, A.P. Ramirez, S.-W. Cheong, B.R. Zegarski, P. Schiffer, and J. Zaanen, Phys. Rev. B **56**, 5104 (1997).
[14] M. Jaime, H.T. Hardner, M.B. Salamon, M. Rubinstein, P. Dorsey, and D. Emin, Phys. Rev. Lett. **78**, 951 (1997).
[15] P. Matl, N.P. Ong, Y.F. Yan, Y.Q. Li, D. Studebaker, T. Baum, and G. Doubinina, Phys. Rev. B **57**, 10 248 (1998).
[16] C.H. Booth, F. Bridges, G.H. Kwei, J.M. Lawrence, A.L. Cornelius, and J.J. Neumeier, Phys. Rev. B **57**, 10 440 (1998).
[17] D. Louca and T. Egami, Phys. Rev. B **59**, 6193 (1999).
[18] A. Lanzara, N.L. Saini, M. Brunelli, F. Natali, A. Bianconi, P.G. Radaelli, and S. Cheong, Phys. Rev. Lett. **81**, 878 (1998).
[19] Note that for neutron scattering the Mn-O peak in the PDF is negative because of the negative scattering length of Mn. However, for x rays this peak is positive.
[20] Th. Proffen, R.G. DiFrancesco, S.J.L. Billinge, E.L. Brosha, and G.H. Kwei, Phys. Rev. B **60**, 9973 (1999).
[21] P. G. Radaelli (unpublished).
[22] P. M. Chaikin and T. C. Lubensky, *Principles of Condensed Matter Physics* (Cambridge University Press, Cambridge, 1995).
[23] B. E. Warren, *X-ray Diffraction* (Dover, New York, 1990).
[24] C.N.J. Wagner, J. Non-Cryst. Solids **31**, 1 (1978).
[25] T. Egami, in *Local Structure from Diffraction*, edited by S. J. L. Billinge and M. F. Thorpe (Plenum, New York, 1998), p. 1.
[26] V. Petkov, I-K. Jeong, J.S. Chung, M.F. Thorpe, S. Kycia, and S.J.L. Billinge, Phys. Rev. Lett. **83**, 4089 (1999).
[27] W. Ruland, J. Appl. Phys. **15**, 1301 (1964).
[28] Y. Waseda, *The Structure of Non-crystalline Materials* (McGraw-Hill, New York, 1980).
[29] V. Petkov, J. Am. Ceram. Soc. **23**, 387 (1989).
[30] M. D. Sturge, in *Solid State Physics*, edited by F. Seitz, D. Turnbull, and H. Ehrenreich (Academic, New York, 1967), Vol. 20, p. 91.
[31] J.M.D. Coey, M. Viret, and S. von Molnár, Adv. Phys. **48**, 167 (1999).
[32] E. Pollert, S. Krupicka, and E. Kuzwicova, J. Phys. Chem. Solids **43**, 1137 (1996).
[33] J.B.A.A. Ellemans, B. van Laar, K.R. van derVeer, and B.O. Loopstra, J. Solid State Chem. **3**, 328 (1971).
[34] P. Allen and V. Perebeinos (unpublished).
[35] G. H. Kwei, D. N. Argyriou, S. J. L. Billinge, A. C. Lawson, J. J. Neumeier, A. P. Ramirez, M. A. Subramanian, and J. D. Thompson, *Magnetic Ultrathin Films, Multilayers and Surfaces–1997*, edited by J. Tobin, D. Chambliss, D. Kubinski, K. Baimark, P. Dederichs, W. de Jorge, T. Katayama, and A. Sohuhl, MRS Symposia Proceedings No. 475 (Materials Research Society, Pittsburgh, 1997) p. 533.
[36] Th. Proffen and S.J.L. Billinge, J. Appl. Crystallogr. **32**, 572 (1999).
[37] R.D. Shannon, Acta Crystallogr., Sect. A: Cryst. Phys., Diffr., Theor. Gen. Crystallogr. **32**, 751 (1976).
[38] K. Poeppelmeier, M. Leonowicz, J. Scanlon, J. Longo, and W. Yelon, J. Solid State Chem. **45**, 71 (1982).
[39] I-K. Jeong, Th. Proffen, F. Mohiuddin-Jacobs, and S.J.L. Billinge, J. Phys. Chem. A **103**, 921 (1999).
[40] J.B.A.A. Elemans, B. Van Laar, K.R. Van Der Veen, and B.O. Loopstra, J. Solid State Chem. **3**, 238 (1971).
[41] S. Hibble, S. Cooper, A. Hannon, I. Fawcett, and M. Greenblatt, J. Phys.: Condens. Matter **11**, 9221 (1999).
[42] M. Uehara, S. Mori, C.H. Chen, and S.-W. Cheong, Nature (London) **399**, 560 (1999).
[43] S-W. Cheong and C. H. Chen, in *Colossal Magnetoresistance*

and Related Properties, edited by B. Raveau and C. N. R. Rao (World Scientific, Singapore, 1999).
[44] A.P. Ramirez, P. Schiffer, S-W. Cheong, W. Bao, T.T.M. Palstra, P.L. Gammel, D.J. Bishop, and B. Zegarski, Phys. Rev. Lett. **76**, 3188 (1996).
[45] R. Kilian and G. Khaliullin, Phys. Rev. B **60**, 13 458 (1999).
[46] S. J. L. Billinge, in *Physics of Manganites*, edited by T. A. Kaplan and S. D. Mahanti (Kluwer Academic, New York, 1999), p. 201.
[47] S. Yunoki, J. Hu, A.L. Malvezzi, A. Moreo, N. Furukawa, and E. Dagotto, Phys. Rev. Lett. **80**, 845 (1998).
[48] M. Jaime and M. B. Salamon, in *Physics of Manganites* (Ref. 46), p. 243.